




Thickness dependent itinerant ferromagnetism in ultrathin Ba-doped SrRuO₃ films

Zeeshan Ali ^{1,*}, Mohammad Saghayezhian,¹ Prahald Siwakoti ^{1,2}, Roshan Nepal,¹ and Jiandi Zhang ^{1,3,†}

¹Department of Physics & Astronomy, Louisiana State University, Baton Rouge, Louisiana 70803, USA

²Department of Physics & Astronomy, University of Tennessee, Knoxville, Tennessee 37996, USA

³Beijing National Laboratory for Condensed Matter Physics, Institute of Physics, Chinese Academy of Sciences, Beijing 100190, People's Republic of China



(Received 22 December 2022; accepted 12 May 2023; published 30 May 2023)

The electronic and magnetic properties in ABO_3 perovskite oxides are extremely sensitive to lattice structure, but also to dimensionality, such as the thickness in thin film-form. Here, we report the thickness-dependent electromagnetic properties of ultrathin epitaxially stabilized $Sr_{1-x}Ba_xRuO_3$ ($x = 0.08, 0.2$) thin films on a $SrTiO_3$ (001) substrate. The results reveal that the barium doping ($0.08 \leq x \leq 0.20$) reduces RuO_6 orthorhombic distortions existing in $SrRuO_3$ and induces a tetragonal distortion, as evidenced by out-of-plane lattice expansion. A metal-to-insulator transition, accompanied by a ferromagnetic to nonmagnetic transition occurs with reducing film thickness from 10 to 3 unit cells for both $x = 0.08$ and 0.2, regardless of the doping level. The results suggest that the effects of compositional vacancies and surface/interface contributions introduced via dimensional confinement are more dominant than A -site chemical disorder or structural distortion for the loss of metallicity and ferromagnetism in ultra-thin epitaxial films.

DOI: [10.1103/PhysRevMaterials.7.054408](https://doi.org/10.1103/PhysRevMaterials.7.054408)

I. INTRODUCTION

Among complex oxides (ABO_3), it is well known that B -site transition-metal dictates the functional properties [1–3]. Minor modifications brought via changing the octahedral environment, and bond symmetry can modify the intricate coupling between structure and electronic spin degrees of freedom, leading to emergent properties [2,4]. One typical example is $4d$ perovskite ruthenates ($ARuO_3$), where varying the A -site isovalent substitution from calcium to strontium to barium not only triggers modified crystal structures, but also affects magnetic ground states [5–10]. In bulk $Sr_{1-x}Ca_xRuO_3$ and the thin-film family, the compound retains orthorhombicity, though ferromagnetism ($x = 0$) evolves to paramagnetism ($x \approx 0.7$) due to altered fermiology [5–8]. On the other hand, the barium placement at the strontium site drives a cubic structure but lowers the Curie temperature (T_C) to 60 K for the final member: $BaRuO_3$ in the bulk $Sr_{1-x}Ba_xRuO_3$ series [5,6]. For the $Sr_{1-x}Ba_xRuO_3$ thin films, using strain engineering, the tuning of crystal symmetry from the orthorhombic to the cubic-like phase without octahedral rotations, as well as modification of perpendicular magnetic anisotropy and magnetization dynamics, have been recently reported [11]. Such tuning of transition-metal perovskite oxides for emergent functionalities via film epitaxy and heterostructure engineering is at the forefront of material science. Through epitaxial strain [12–20], interfacial effects [21–25], superlattices [26–30], confinement [31–35], doping/implantation [36–38], and dimensionality [39–43], a delicate equilibrium among structure, spin, charge, and orbital

degrees of freedom could be manipulated, leading to novel properties that are different from the bulk.

Gaining insight into the nature of electronic and magnetic properties of the $Sr_{1-x}Ba_xRuO_3$ ($x = 0.08, 0.2$) thin-film family in an ultrathin regime, especially in a range of only a few unit-cell (u.c.) thicknesses, is the focus of this work. The barium doping into an ultrathin epitaxial $SrRuO_3$ lattice introduces a local RuO_6 octahedra elongation, while the nature of electron transport and itinerant magnetism shows stability against barium-induced local structural distortion. The placement of the Ba^{2+} ion at the Sr^{2+} site introduces randomized cation disorder; however, a thickness-driven metal-to-insulator transition (MIT) and nonmagnetic state occurs at the same thickness of 3 u.c. for both doping levels ($x = 0.08, 0.2$). The results indicate that disordering effects such as compositional vacancies and surface/interface contributions introduced via dimensional confinement are more significant than the perturbative effects of local structural distortion and cation disorder, leading to MIT and a nonmagnetic state.

II. EXPERIMENTAL DETAILS

The $Sr_{1-x}Ba_xRuO_3$ ($x = 0.08, 0.2$) thin films were grown by pulse laser deposition using a KrF excimer laser with a 10-Hz repetition rate and an energy density of ~ 1 J/cm². The TiO_2 -terminated $SrTiO_3$ (001) substrates were employed, whereas thin films were grown at 700°C under an oxygen pressure of 100 mTorr and cooled down at 100 mTorr. The film thickness was monitored by *in situ* reflection high-energy electron diffraction (RHEED). The film's crystal structure was characterized by using a PanAnalytical X'Pert thin-film diffractometer. Electron transport measurements were performed via the quantum design physical property measurement

*zee89ali@gmail.com

†jiandiz@iphy.ac.cn

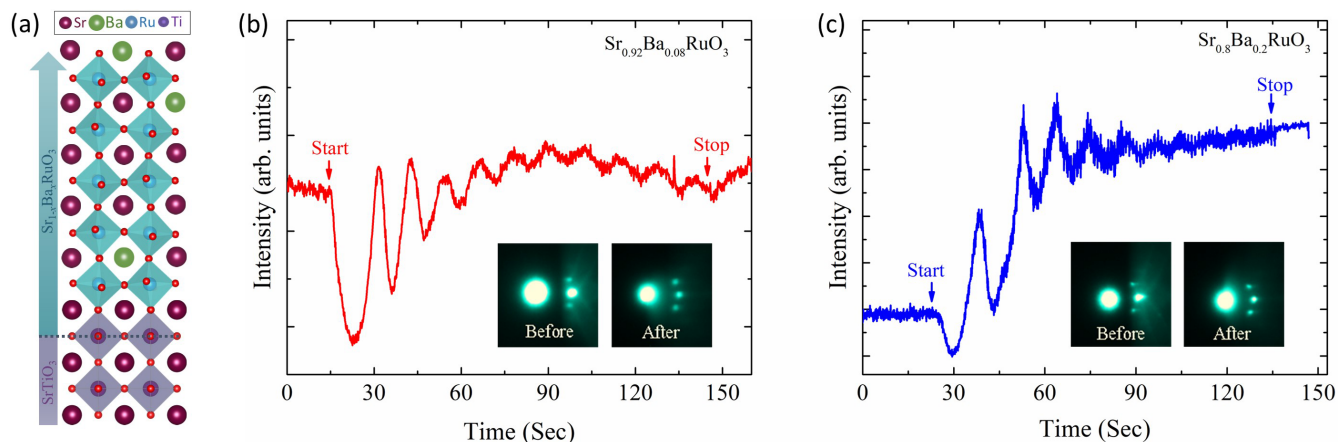


FIG. 1. (a) Schematic representation of $\text{Sr}_{1-x}\text{Ba}_x\text{RuO}_3$ film grown on a SrTiO_3 (001) substrate. (b) and (c) Time-dependent RHEED intensity profile of the (0,0) spot for $\text{Sr}_{1-x}\text{Ba}_x\text{RuO}_3$ ($x = 0.08, 0.2$) thin films with a thickness of 10 u.c. The inset in (b) and (c) shows the specular spot diffraction pattern before and after film growth.

system in a four-probe configuration. The sample magnetization was studied by using a quantum design superconducting quantum interference device, reciprocating sample option.

III. RESULTS AND DISCUSSION

A. Film epitaxy

Figure 1(a) shows a schematic of the $\text{Sr}_{1-x}\text{Ba}_x\text{RuO}_3$ thin film epitaxy on a TiO_2 -terminated SrTiO_3 (001) substrate, whereas Fig. 1(b) and 1(c) displays *in situ* RHEED data of 10 u.c. $\text{Sr}_{1-x}\text{Ba}_x\text{RuO}_3$ ($x = 0.08$ and 0.2) films. Figure 1(b) and 1(c) displays the RHEED images of both the substrate and films along with the RHEED spot intensities vs. growth time. The RHEED image of the SrTiO_3 substrate [Fig. 1(b) and 1(c), inset] before deposition shows high-intensity specular spots and Kikuchi lines, verifying high substrate quality. Figure 1(b) and 1(c) advocates that diffraction intensity of the (0,0) spot oscillated in a layer-by-layer mode for few initial layers. However, as the film grows thicker, the specular spot intensity begins to saturate, reflecting a preference toward step-flow epitaxy. In the step-flow growth, instead of forming new nuclei on the terrace, the adatoms like to attach to the step edges, leading to the advancement of the step edge along the terraces. The step-flow growth mechanism in ruthenates leads to the formation of high-quality epitaxial films with a well-defined crystal structure and surface morphology. This is also evident in the after-growth specular diffraction spots [Fig. 1(b) and 1(c), inset]. Overall, both the time-dependent intensity profile of RHEED spots and streaky RHEED pattern after film growth point to a flat crystalline surface having two-dimensional growth typically observed for ruthenate perovskites.

B. Crystal structure

The crystal structure of $\text{Sr}_{1-x}\text{Ba}_x\text{RuO}_3$ thin films was investigated via x-ray diffraction (XRD). Figure 2(a) shows a coupled (θ - 2θ) x-ray scan around the (002) SrTiO_3 reflection for 10-u.c. $\text{Sr}_{1-x}\text{Ba}_x\text{RuO}_3$ ($x = 0.08, 0.2$) thin films. XRD showed only substrate and film peaks, confirming coher-

ent film epitaxy and excellent crystalline quality [Fig. 2(a)]. The films maintain pseudocubic structural symmetry while the out-of-plane pseudocubic lattice parameter increases systematically with increasing barium substitution from 0.08 to 0.2, i.e., a barium doping-dependent tetragonal elongation compared to the SrRuO_3 films [11,19,20,36,44–46]. The $\text{Sr}_{0.92}\text{Ba}_{0.08}\text{RuO}_3$ film shows an out-of-plane lattice parameter of $c_{pc} = 4.029 \pm 0.05$ (bulk $c_{pc} = 3.944$ Å), which enhances slightly to $c_{pc} = 4.076 \pm 0.08$ (bulk $c_{pc} = 3.968$ Å) for the $\text{Sr}_{0.8}\text{Ba}_{0.2}\text{RuO}_3$ film. The enhancement in c_{pc} compared to bulk counterparts is due to compressive strain, which enforces the in-plane parameter to undergo compression to match the SrTiO_3 (3.905 Å), while the out-of-plane constant increases.

To understand the crystal structure further, we performed reciprocal space mapping (RSM) around $(103)_{pc}$ reflections for 10-u.c. $\text{Sr}_{0.92}\text{Ba}_{0.08}\text{RuO}_3$ and $\text{Sr}_{0.8}\text{Ba}_{0.2}\text{RuO}_3$ films [Fig. 2(b) and 2(c)]. The RSM is obtained around the $(103)_{pc}$ SrTiO_3 reflection with a φ angle of $0^\circ, 90^\circ, 180^\circ$, and 270° . We observe that the $\text{Sr}_{0.92}\text{Ba}_{0.08}\text{RuO}_3$ [Fig. 2(b)] film shows matching Q_z reflection for the family of $(103)_{pc}$ reflections, indicating a tetragonal symmetry [16,45,47]. Likewise, the $\text{Sr}_{0.8}\text{Ba}_{0.2}\text{RuO}_3$ film also holds a tetragonal symmetry [Fig. 2(c)]. Moreover, the trend of identical Q_x values of SrTiO_3 endorses the epitaxially strained nature of films, ensuring excellent quality.

C. Thickness-dependent electric transport

Resistivity as a function of temperature for thicknesses ranging from 10 to 3 u.c. for the $\text{Sr}_{1-x}\text{Ba}_x\text{RuO}_3$ ($x = 0.08, 0.2$) series is shown in Fig. 3(a) and 3(b). First, we observe that increasing the barium doping from 0.08 to 0.2 results in an increase of the resistivity value at room temperature for films with the same thickness (10, 7 u.c.), suggesting a cation disorder effect. However, such resistivity enhancement posts an insignificant impact on $\rho(T)$ functional dependencies (discussed later). More importantly, film thickness reduction results in a MIT at the same thickness of 3 u.c. for both doping levels ($x = 0.08, 0.2$). We can divide the electron transport [Fig. 3(a) and 3(b)] into three electronic regimes as the film

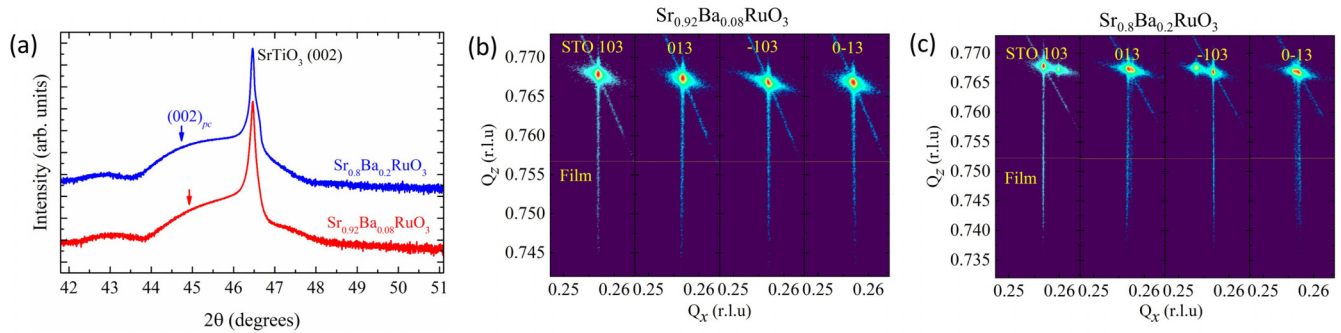


FIG. 2. (a) Coupled $(\theta-2\theta)$ x-ray scan of $\text{Sr}_{1-x}\text{Ba}_x\text{RuO}_3$ ($x = 0.08, 0.2$) films around (002) SrTiO_3 . (b) and (c) Reciprocal space mapping about the $(103)_{pc}$ reflections for $\text{Sr}_{0.92}\text{Ba}_{0.08}\text{RuO}_3$ and $\text{Sr}_{0.8}\text{Ba}_{0.2}\text{RuO}_3$ films, respectively.

thickness is systematically varied for the $\text{Sr}_{1-x}\text{Ba}_x\text{RuO}_3$ ($x = 0.08, 0.2$) series. First, as shown in Fig. 3(a), the 10-u.c. film of $\text{Sr}_{0.92}\text{Ba}_{0.08}\text{RuO}_3$, which has the lowest room-temperature resistivity among the different thicknesses of the films, displays metallic behavior characterized by $d\rho/dT > 0$ down to the lowest temperature of 5 K. A clear kink in $\rho(T)$ curve appears at around ~ 133 K, concurring with the magnetic phase transition (discussed later), similar to that observed in the bulk crystal of SrRuO_3 [48,49]. Decreasing the film thickness to an intermediate region (7 and 5 u.c.) triggers amplification in room-temperature resistivity, whereas the films exhibit a metallic behavior only at high temperatures [Fig. 3(a)]. Specifically, the low-temperature resistivity exhibits a negative slope ($d\rho/dT < 0$) below $T_{MIT} \sim 23$ K in 7-u.c. film, thus showing nonmetallic character [T_{MIT} is marked with an arrow in Fig. 3(a)]. The reduction of film thickness to 5 u.c. not only increases film resistivity, but also shifts the resistivity upturn to the higher temperature of $T_{MIT} \sim 68$ K. The existence of such a resistivity upturn with a minimum is a sign that the system is at the edge of the metal-insulator transition

[39–43,50]. Finally, when the film thickness is further reduced to 3 u.c., an insulating behavior ($d\rho/dT < 0$) is observed in the entire temperature range.

The three kinds of transport regimes are also preserved in $\text{Sr}_{0.8}\text{Ba}_{0.2}\text{RuO}_3$ films, even though the increase in barium doping ($x = 0.2$) results in a minor increase in room-temperature resistivity [Fig. 3(b)]. Noticeably, a thickness-dependent MIT occurs at an identical thickness of 3 u.c. regardless of barium doping levels ($x = 0.08, 0.2$). The 10 u.c. of the $\text{Sr}_{0.8}\text{Ba}_{0.2}\text{RuO}_3$ film shows metallicity down to the lowest temperature, while the intermediate-region (7 and 5 u.c.) films retain a high-temperature metallicity, yet resistivity upturn arises at low temperatures, near $T_{MIT} \sim 19$ K and $T_{MIT} \sim 55$ K, respectively. Below this thickness, a fully insulating regime ascends as realized for 3-u.c. film. Thus, we conclude that the $\text{Sr}_{1-x}\text{Ba}_x\text{RuO}_3$ ($x = 0.08, 0.2$) series undergoes a MIT with films thinner than or equal to 3 u.c., regardless of the barium doping level ($x = 0.08, 0.2$). This is analogous to the results of SrRuO_3 films grown on SrTiO_3 (001), where MIT occurs near 3 u.c. [39–41].

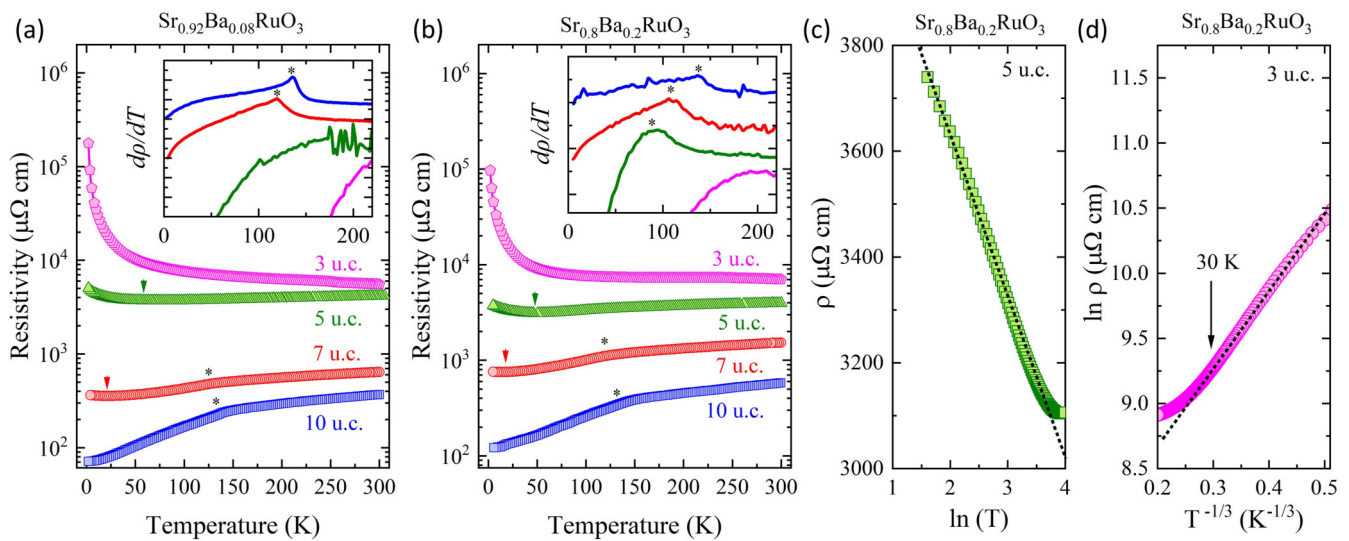


FIG. 3. (a) and (b) $\text{Sr}_{1-x}\text{Ba}_x\text{RuO}_3$ ($x = 0.08, 0.2$) films' resistivity as a function of temperature for different thicknesses. The insets in (a) and (b) are a temperature-dependent resistivity derivative ($d\rho/dT$) plotted against temperature (T). In (a) and (b), the T_{MIT} and T_C are marked with arrows and asterisks, respectively. (c) Resistivity as function of $\ln(T)$ for 5-u.c. $\text{Sr}_{0.8}\text{Ba}_{0.2}\text{RuO}_3$ film. The black dotted line is the linear fit. (d) Logarithm of resistivity plotted versus $T^{-1/3}$ (two-dimensional Mott VRH) for 3-u.c. $\text{Sr}_{0.8}\text{Ba}_{0.2}\text{RuO}_3$ film. The black dotted line is the linear fit.

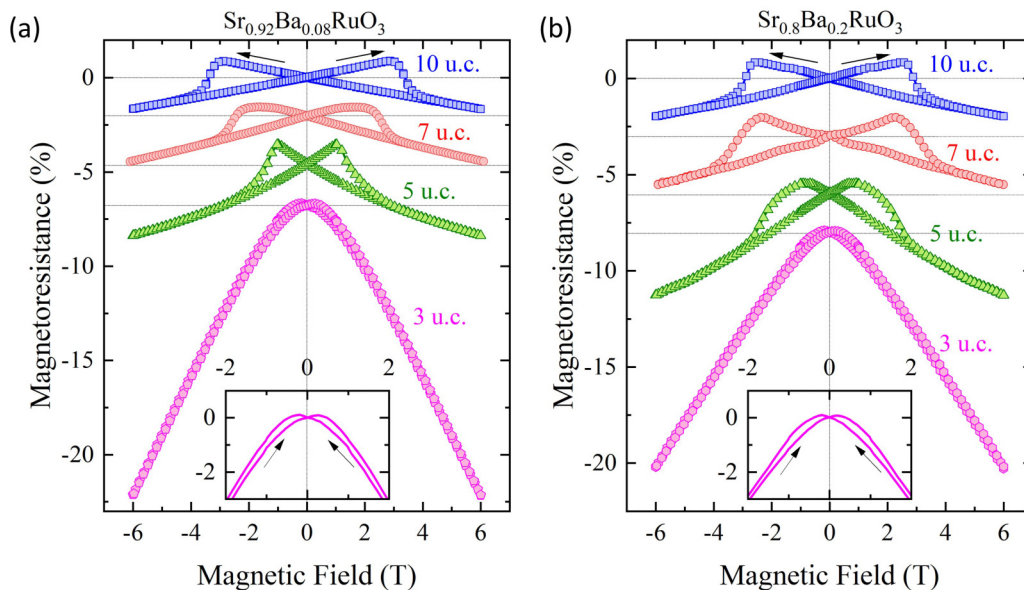


FIG. 4. The MR of (a) $\text{Sr}_{0.92}\text{Ba}_{0.08}\text{RuO}_3$ and (b) $\text{Sr}_{0.8}\text{Ba}_{0.2}\text{RuO}_3$ films measured at 5 K with a magnetic field applied along the out-of-plane direction. The MR curves are offset to avoid the overlap. The inset in (a) and (b) shows low-field MR of 3-u.c. $\text{Sr}_{1-x}\text{Ba}_x\text{RuO}_3$ ($x = 0.08, 0.2$), highlighting the weak MR hysteresis.

The resistivity upturn is an indicator for MIT and has been observed in several oxide films [19,33,39–43,50–52]. In the ultrathin-film regime, the effect of weak localization induced via disorder could trigger a resistivity upturn. The presence of disorder/defects results in the amplification of backscattering of the conducting electrons, leading to the interference of electronic wavefunctions and thus causing larger resistivity films [40–43,50–55]. The phenomenon of weak localization in two-dimensional systems results in a quantum correction to conductivity with a characteristic logarithmic $[\ln(T)]$ dependence. Apparently, the signatures of weak localization-induced resistivity minima are prevailing in the $\text{Sr}_{1-x}\text{Ba}_x\text{RuO}_3$ ($x = 0.08, 0.2$) series at a film thickness of 5 u.c. Specifically, the 5-u.c. $\text{Sr}_{0.8}\text{Ba}_{0.2}\text{RuO}_3$ film resistivity reveals a $\ln(T)$ dependence in a low-temperature regime (< 50 K), as shown in Fig. 3(c). Meanwhile, the effect of electron-electron correlations can also produce a $\ln(T)$ dependence, considering the fact that electron-electron correlations might be enhanced in low-dimensional systems [10,33,56]. However, one can differentiate the effect of electron-electron correlations from weak localization via magnetoresistance (MR) measurements, as discussed later.

The MR of $\text{Sr}_{1-x}\text{Ba}_x\text{RuO}_3$ ($x = 0.08, 0.2$) films is shown in Fig. 4(a) and 4(b). The MR is defined as $\text{MR} = \{\rho(H) - \rho(0)\}/\rho(0)$, where $\rho(0)$ and $\rho(H)$ are resistivities in the absence and presence of an external magnetic field, respectively. Here, the magnetic field (H) is applied along the film-normal direction. For films under the study, both doping levels [$\text{Sr}_{1-x}\text{Ba}_x\text{RuO}_3$ ($x = 0.08, 0.2$)] characteristically show identical MR behavior at 5 K. The MR of 10 to 5 u.c. ($x = 0.08, 0.2$) films displays a “butterfly” hysteretic MR, a signature of ferromagnetic (FM) ordering. In contrast, for 3 u.c., the butterfly MR becomes very weak (nearly vanishing), indicating a very weak magnetic system [Fig. 4(a) and 4(b), inset]. At the same time, the MR enhances monotonically with a reduction in film dimensionality, which could be associated

with charge localization. Similar behavior has been observed in the CaRuO_3 films, though without long-range magnetic ordering [35].

The magnetoresistance can be valuable to distinguish the contribution of weak localization from electron-electron correlation in resistivity upturn. The presence of the external magnetic-field presence can demolish the electronic wavefunctions coherence by dephasing the two wavefunctions that are traveling in clockwise and anticlockwise trajectories, leading to destructive interference and abolishment of weak localization—hence a negative magnetoresistance [42,53,57–59]. In contrast, the electronic correlation effect triggers a positive magnetoresistance [53,57,58]. As seen in Fig. 4(d) and 4(e), the 5-u.c. films ($x = 0.08, 0.2$) holding a resistivity minimum show mainly negative magnetoresistance, confirming that the resistivity minimum arises due to disorder-induced localization.

As mentioned earlier, the dimensional confinement in the $\text{Sr}_{1-x}\text{Ba}_x\text{RuO}_3$ ($x = 0.08, 0.2$) films results in a progressive evolution in the transport behavior from a metallic region (10 to 7 u.c.) to a weak localization state (5 u.c.) to a highly insulating behavior at 3 u.c. As shown in Fig. 3(d), the low-temperature resistivity of insulating 3-u.c. $\text{Sr}_{0.8}\text{Ba}_{0.2}\text{RuO}_3$ film (taken as an example) exhibits two-dimensional variable range-hopping (VRH) conduction characteristics: $\ln(\rho) \propto T^{-1/3}$.

Generally, in the variable range-hopping model fitting as employed in our case, we have the relation $\rho(T) = \rho_0 \exp[(\frac{T_M}{T})^{\frac{1}{d+1}}]$, where $d = 1, 2, 3$ is system dimensionality and T_M is the Mott characteristic temperature [60,61]. In Mott-type VRH, the Coulomb interaction between hopping sites is ignored, thus the density of states near the Fermi level is considered a constant. In our case, we have $d = 2$, so we are plotting a linear equation of the form $\ln(T) \propto (\frac{T_M}{T})^{\frac{1}{3}}$. Thus, using the slope, one can get Mott characteristic temperature

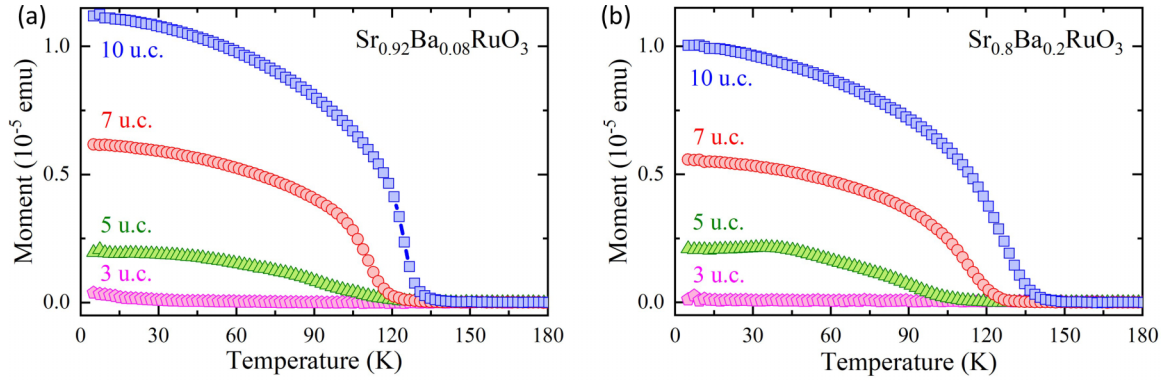


FIG. 5. Magnetization versus temperature of (a) $\text{Sr}_{0.92}\text{Ba}_{0.08}\text{RuO}_3$ and (b) $\text{Sr}_{0.8}\text{Ba}_{0.2}\text{RuO}_3$ films measured along the out-of-plane direction.

(one gets $T_M \sim 500$ K from the linear fit), which in turn could be used to calculate the density of states or other localization parameters using the relationship $T_M = \frac{\beta_M}{k_B g(\epsilon_F) \xi^d}$. Here, T_M is the Mott characteristic temperature signifying degree of disorder, $g(\epsilon_F)$ is the density of states, ξ is the localization length, β_M is a constant, k_B is the Boltzmann constant, and d is system dimensionality with values 1, 2, 3.

The results described earlier suggest that the observed thickness-dependent MIT is administered by disorder-driven Anderson localization [60–63]. Disorder refers to random fluctuations or variations due to the presence of impurities or defects in a system that breaks the electronic wave symmetry and causes the electronic wavefunctions to become localized, leading to the suppression of electrical conductivity. In our case here, the barium substitution introduces A-site cation disorder as well as local structural distortion. At the same time, reducing the film thickness can introduce and amplify additional disorder effects such as compositional (ruthenium and oxygen) vacancies, and surface/interface contributions [34,38,46,64–67]. Compared to the chemical disorder at the A-site by barium doping, the disorder induced by condensing the film thickness can be more severe in the activation of electron localization since, for example, the appearance of compositional (ruthenium and oxygen) vacancies can drastically affect the p - d orbital hybridization in the building block RuO_6 of perovskite oxides. This is likely the reason that the films exhibit the same critical thickness for MIT regardless of different barium doping levels [10,34,68,69].

D. Thickness-dependent magnetization

To study the magnetic properties of $\text{Sr}_{1-x}\text{Ba}_x\text{RuO}_3$ ($x = 0.08, 0.2$) thin films, we performed superconducting quantum interference device magnetometry for films with different thicknesses ($t = 3, 5, 7, 10$ u.c.). For measuring the magnetization versus temperature [$M(T)$], the films were cooled down under a field of 2000 Oe to 5 K, and then their $M(T)$ was measured during warmup with a field of 100 Oe. Figure 5(a) shows the $M(T)$ of $\text{Sr}_{0.92}\text{Ba}_{0.08}\text{RuO}_3$ films with thicknesses varying from 3 to 10 u.c. The $M(T)$ shows that thicker film (10 u.c.) holds a paramagnetic (PM) to FM transition at 136 ± 4 K [almost the same as the kink position; ~ 133 K in the $\rho(T)$ curve shown in Fig. 3(a)]. However, the systematic reduction of film thickness suppresses the FM order and T_C ,

ending with the 3-u.c. film nonmagnetic. These observations suggest that thickness-dependent transition from a FM to a non-FM state occurs at a 3-u.c. thickness. Likewise, the $M(T)$ data of $\text{Sr}_{0.8}\text{Ba}_{0.2}\text{RuO}_3$ films with varying thickness exhibit behavior similar to that of $\text{Sr}_{0.92}\text{Ba}_{0.08}\text{RuO}_3$ films. Overall, the observations suggest that a thickness-dependent transition from a FM to non-FM state occurs at a 3-u.c. thickness in the $\text{Sr}_{1-x}\text{Ba}_x\text{RuO}_3$ ($x = 0.08, 0.2$) series.

Lastly, we have plotted the T_C as functions of film thickness for $\text{Sr}_{1-x}\text{Ba}_x\text{RuO}_3$ ($x = 0.08, 0.2$) films extracted from Fig. 5. It can be seen that as the film thickness is reduced to 3 u.c., the FM order is diminished without a clear onset of magnetism (no measurable the T_C either) for both doping levels. At the same time, we have also plotted the T_{MIT} in Fig. 6. The T_{MIT} is extracted from Fig. 3(a) and 3(b) and is marked by arrows. The transport data in Fig. 3(a) and 3(b) have shown that 3-u.c. films are insulating in a measured temperature range (no measurable T_{MIT} is observed). Thus, the emergence of a non-FM state coincides with the insulating state. This implies that the metallicity and FM ordering go parallel to each other, which is expected for an itinerant system such as $\text{Sr}_{1-x}\text{Ba}_x\text{RuO}_3$ ($x = 0.08, 0.2$). The trend of the T_C and T_{MIT} is consistent with the reports on SrRuO_3 films, where films are found to be nonmagnetic and insulating near 2 to 3 u.c. [39–41,70].

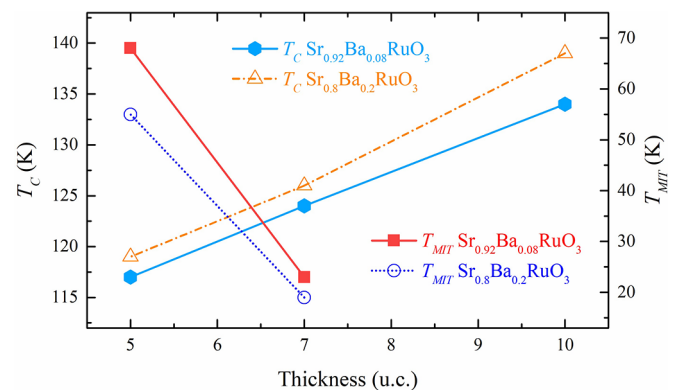


FIG. 6. The T_C and T_{MIT} plotted against film thickness for series of $\text{Sr}_{0.92}\text{Ba}_{0.08}\text{RuO}_3$ and $\text{Sr}_{0.8}\text{Ba}_{0.2}\text{RuO}_3$ films within the measured temperature range (5 to 300 K).

IV. CONCLUSION

To summarize, we have studied the thickness-dependent electromagnetic properties of ultrathin $\text{Sr}_{1-x}\text{Ba}_x\text{RuO}_3$ ($x = 0.08, 0.2$) thin films grown on SrTiO_3 (001). The study reveals that barium doping induces out-of-plane lattice expansion, yet itinerant magnetism of SrRuO_3 displays robustness against barium doping. Notably, the electron transport reveals that barium-doped SrRuO_3 films ($x = 0.08, 0.2$) undergo a MIT at 3 u.c., while above this thickness, films are metallic. The emergence of an insulating state coincides with a non-FM state. The outcomes highlight that reducing the film thickness

introduces and amplifies the disordering effects such as compositional (ruthenium and oxygen) variation, and surface/interface contributions, which are dominant compared to the barium-induced effects of cation disorder and local structural distortion, triggering the metal-insulator and ferromagnetic-nonmagnetic transitions in ultrathin epitaxial films.

ACKNOWLEDGMENT

This work is primarily supported by the US Department of Energy (DOE) (Grant No. DOE DE-SC0002136).

-
- [1] C. H. Ahn, A. Bhattacharya, M. Di Ventura, J. N. Eckstein, C. D. Frisbie, M. E. Gershenson, A. M. Goldman, I. H. Inoue, J. Mannhart, A. J. Millis, A. F. Morpurgo, D. Natelson, and J. M. Triscone, Electrostatic modification of novel materials, *Rev. Mod. Phys.* **78**, 1185 (2006).
- [2] J. M. Rondinelli, S. J. May, and J. W. Freeland, Control of octahedral connectivity in perovskite oxide heterostructures: An emerging route to multifunctional materials discovery, *MRS Bull.* **37**, 261 (2012).
- [3] A. Bhattacharya and S. J. May, Magnetic oxide heterostructures, *Annu. Rev. Mater. Res.* **44**, 65 (2014).
- [4] H. Y. Hwang, Y. Iwasa, M. Kawasaki, B. Keimer, N. Nagaosa, and Y. Tokura, Emergent phenomena at oxide interfaces, *Nat. Mater.* **11**, 103 (2012).
- [5] C. Q. Jin, J. S. Zhou, J. B. Goodenough, Q. Q. Liu, J. G. Zhao, L. X. Yang, Y. Yu, R. C. Yu, T. Katsura, A. Shatskiy, and E. Ito, High-pressure synthesis of the cubic perovskite BaRuO_3 and evolution of ferromagnetism in ARuO_3 ($A = \text{Ca}, \text{Sr}, \text{Ba}$) ruthenates, *Proc. Natl. Acad. Sci. USA* **105**, 7115 (2008).
- [6] J. G. Cheng, J. S. Zhou, and J. B. Goodenough, Lattice effects on ferromagnetism in perovskite ruthenates, *Proc. Natl. Acad. Sci. USA* **110**, 13312 (2013).
- [7] L. T. Nguyen, M. Abeykoon, J. Tao, S. Lapidus, and R. J. Cava, Long-range and local crystal structures of the $\text{Sr}_{1-x}\text{Ca}_x\text{RuO}_3$ perovskites, *Phys. Rev. Mater.* **4**, 034407 (2020).
- [8] G. Cao, S. McCall, M. Shepard, J. Crow, and R. Guertin, Thermal, magnetic, and transport properties of single-crystal $\text{Sr}_1\text{Ca}_x\text{RuO}_3$ ($0 < x < 1.0$), *Phys. Rev. B* **56**, 321 (1997).
- [9] I. I. Mazin and D. J. Singh, Electronic structure and magnetism in Ru-based perovskites, *Phys. Rev. B* **56**, 2556 (1997).
- [10] J. M. Rondinelli, N. M. Caffrey, S. Sanvito, and N. A. Spaldin, Electronic properties of bulk and thin film SrRuO_3 : Search for the metal-insulator transition, *Phys. Rev. B* **78**, 155107 (2008).
- [11] Z. Ali, Z. Wang, A. R. Mazza, M. Saghayezhian, R. Nepal, T. Z. Ward, Y. Zhu, and J. Zhang, Tuning structural, transport and magnetic properties of epitaxial SrRuO_3 through Ba substitution, *Phys. Rev. B* **107**, 144405 (2023).
- [12] J. H. Haeni, P. Irvin, W. Chang, R. Uecker, P. Reiche, Y. L. Li, S. Choudhury, W. Tian, M. E. Hawley, B. Craigo, A. K. Tagantsev, X. Q. Pan, S. K. Streiffer, L. Q. Chen, S. W. Kirchoefer, J. Levy, and D. G. Schlom, Room-temperature ferroelectricity in strained SrTiO_3 , *Nature (London)* **430**, 758 (2004).
- [13] W. Lu, W. Song, P. Yang, J. Ding, G. M. Chow, and J. Chen, Strain Engineering of octahedral rotations and physical properties of SrRuO_3 films, *Sci. Rep.* **5**, 10245 (2015).
- [14] D. Kan, R. Aso, H. Kurata, and Y. Shimakawa, Epitaxial strain effect in tetragonal SrRuO_3 thin films, *J. Appl. Phys.* **113**, 173912 (2013).
- [15] A. Vailionis, H. Boschker, W. Siemons, E. P. Houwman, D. H. A. Blank, G. Rijnders, and G. Koster, Misfit strain accommodation in epitaxial ABO_3 perovskites: Lattice rotations and lattice modulations, *Phys. Rev. B* **83**, 064101 (2011).
- [16] A. Vailionis, W. Siemons, and G. Koster, Room temperature epitaxial stabilization of a tetragonal phase in ARuO_3 ($A = \text{Ca}$ and Sr) thin films, *Appl. Phys. Lett.* **93**, 051909 (2008).
- [17] J. P. Ruf, H. Paik, N. J. Schreiber, H. P. Nair, L. Miao, J. K. Kawasaki, J. N. Nelson, B. D. Faeth, Y. Lee, B. H. Goodge, B. Pamuk, C. J. Fennie, L. F. Kourkoutis, D. G. Schlom, and K. M. Shen, Strain-stabilized superconductivity, *Nat. Commun.* **12**, 59 (2021).
- [18] D. G. Schlom, L. Q. Chen, C. J. Fennie, V. Gopalan, D. A. Muller, X. Pan, R. Ramesh, and R. Uecker, Elastic strain engineering of ferroic oxides, *MRS Bull.* **39**, 118 (2014).
- [19] P. Siwakoti, Z. Wang, M. Saghayezhian, D. Howe, Z. Ali, Y. Zhu, and J. Zhang, Abrupt orthorhombic relaxation in compressively strained ultra-thin SrRuO_3 films, *Phys. Rev. Mater.* **5**, 114409 (2021).
- [20] Y. K. Wakabayashi, S. Kaneta-Takada, Y. Krockenberger, Y. Taniyasu, and H. Yamamoto, Wide-range epitaxial strain control of electrical and magnetic properties in high-quality SrRuO_3 films, *ACS Appl. Electron. Mater.* **3**, 2712 (2021).
- [21] P. Zubko, S. Gariglio, M. Gabay, P. Ghosez, and J.-M. Triscone, Interface physics in complex oxide heterostructures, *Annu. Rev. Condens. Matter Phys.* **2**, 141 (2011).
- [22] A. Ohtomo and H. Y. Hwang, A high-mobility electron gas at the $\text{LaAlO}_3/\text{SrTiO}_3$ heterointerface, *Nature (London)* **427**, 423 (2004).
- [23] H. Lee, N. Campbell, J. Lee, T. J. Asel, T. R. Paudel, H. Zhou, J. W. Lee, B. Noesges, J. Seo, B. Park, L. J. Brillson, S. H. Oh, E. Y. Tsymlal, M. S. Rzchowski, and C. B. Eom, Direct observation of a two-dimensional hole gas at oxide interfaces, *Nat. Mater.* **17**, 231 (2018).
- [24] K. S. Takahashi, M. Kawasaki, and Y. Tokura, Interface ferromagnetism in oxide superlattices of $\text{CaMnO}_3/\text{CaRuO}_3$, *Appl. Phys. Lett.* **79**, 1324 (2001).
- [25] N. Reyren, S. Thiel, A. D. Caviglia, L. Fitting Kourkoutis, G. Hammerl, C. Richter, C. W. Schneider, T. Kopp, A. S. Rüetschi, D. Jaccard, M. Gabay, D. A. Muller, J. M. Triscone, and J. Mannhart, Superconducting interfaces between insulating oxides, *Science* **317**, 1196 (2007).

- [26] A. Bhattacharya, S. J. May, S. G. E. te Velthuis, M. Warusawithana, X. Zhai, B. Jiang, J.-M. Zuo, M. R. Fitzsimmons, S. D. Bader, and J. N. Eckstein, Metal-Insulator Transition and its Relation to Magnetic Structure in $(\text{LaMnO}_3)^{2n}/(\text{SrMnO}_3)^n$ Superlattices, *Phys. Rev. Lett.* **100**, 257203 (2008).
- [27] R. Ramesh and D. G. Schlom, Creating emergent phenomena in oxide superlattices, *Nat. Rev. Mater.* **4**, 257 (2019).
- [28] C. Domínguez, A. B. Georgescu, B. Mundet, Y. Zhang, J. Fowlie, A. Mercy, A. Waelchli, S. Catalano, D. T. L. Alexander, P. Ghosez, A. Georges, A. J. Millis, M. Gibert, and J. M. Triscone, Length scales of interfacial coupling between metal and insulator phases in oxides, *Nat. Mater.* **19**, 1182 (2020).
- [29] H. Boschker, T. Harada, T. Asaba, R. Ashoori, A. V. Boris, H. Hilgenkamp, C. R. Hughes, M. E. Holtz, L. Li, D. A. Muller, H. Nair, P. Reith, X. Renshaw Wang, D. G. Schlom, A. Soukiasian, and J. Mannhart, Ferromagnetism and Conductivity in Atomically Thin SrRuO_3 , *Phys. Rev. X* **9**, 011027 (2019).
- [30] H. Guo, Z. Wang, S. Dong, S. Ghosh, M. Saghayezhian, L. Chen, Y. Weng, A. Herklotz, T. Z. Ward, R. Jin, S. T. Pantelides, Y. Zhu, J. Zhang, and E. W. Plummer, Interface-induced multi-ferroism by design in complex oxide superlattices, *Proc. Natl. Acad. Sci. USA* **114**, E5062 (2017).
- [31] D. Kan, R. Aso, R. Sato, M. Haruta, H. Kurata, and Y. Shimakawa, Tuning magnetic anisotropy by interfacially engineering the oxygen coordination environment in a transition metal oxide, *Nat. Mater.* **15**, 432 (2016).
- [32] Z. Liao, M. Huijben, Z. Zhong, N. Gauquelin, S. Macke, R. J. Green, S. Van Aert, J. Verbeeck, G. Van Tendeloo, K. Held, G. A. Sawatzky, G. Koster, and G. Rijnders, Controlled lateral anisotropy in correlated manganite heterostructures by interface-engineered oxygen octahedral coupling, *Nat. Mater.* **15**, 425 (2016).
- [33] M. Meng, Z. Wang, A. Fathima, S. Ghosh, M. Saghayezhian, J. Taylor, R. Jin, Y. Zhu, S. T. Pantelides, J. Zhang, E. W. Plummer, and H. Guo, Interface-induced magnetic polar metal phase in complex oxides, *Nat. Commun.* **10**, 5248 (2019).
- [34] Z. Ali, Z. Wang, A. O'Hara, M. Saghayezhian, D. Shin, Y. Zhu, S. T. Pantelides, and J. Zhang, Origin of insulating and non-ferromagnetic SrRuO_3 monolayers, *Phys. Rev. B* **105**, 054429 (2022).
- [35] Z. Ali, M. Saghayezhian, Z. Wang, A. O'Hara, D. Shin, W. Ge, Y. T. Chan, Y. Zhu, W. Wu, S. T. Pantelides, and J. Zhang, Emergent ferromagnetism and insulator-metal transition in δ -doped ultrathin ruthenates, *npj Quantum Mater.* **7**, 108 (2022).
- [36] A. Herklotz, A. T. Wong, T. Meyer, M. D. Biegalski, H. N. Lee, and T. Z. Ward, Controlling octahedral rotations in a perovskite via strain doping, *Sci. Rep.* **6**, 26491 (2016).
- [37] E. Skoropata, A. R. Mazza, A. Herklotz, J. M. Ok, G. Eres, M. Brahlek, T. R. Charlton, H. N. Lee, and T. Z. Ward, Post-synthesis control of Berry phase driven magnetotransport in SrRuO_3 films, *Phys. Rev. B* **103**, 085121 (2021).
- [38] C. Wang, C. Chang, A. Herklotz, C. Chen, F. Ganss, U. Kentsch, D. Chen, X. Gao, Y. Zeng, O. Hellwig, M. Helm, S. Gemming, Y. Chu, and S. Zhou, Topological Hall effect in single thick SrRuO_3 layers induced by defect engineering, *Adv. Electron. Mater.* **6**, 2000184 (2020).
- [39] J. Xia, W. Siemons, G. Koster, M. R. Beasley, and A. Kapitulnik, Critical thickness for itinerant ferromagnetism in ultrathin films of SrRuO_3 , *Phys. Rev. B* **79**, 140407(R) (2009).
- [40] X. Shen, X. Qiu, D. Su, S. Zhou, A. Li, and D. Wu, Thickness-dependent metal-insulator transition in epitaxial SrRuO_3 ultrathin films, *J. Appl. Phys.* **117**, 015307 (2015).
- [41] Y. J. Chang, C. H. Kim, S.-H. Phark, Y. S. Kim, J. Yu, and T. W. Noh, Fundamental Thickness Limit of Itinerant Ferromagnetic SrRuO_3 Thin Films, *Phys. Rev. Lett.* **103**, 057201 (2009).
- [42] R. Scherwitzl, S. Gariglio, M. Gabay, P. Zubko, M. Gibert, and J. M. Triscone, Metal-Insulator Transition in Ultrathin LaNiO_3 Films, *Phys. Rev. Lett.* **106**, 246403 (2011).
- [43] G. Wang, Z. Wang, M. Meng, M. Saghayezhian, L. Chen, C. Chen, H. Guo, Y. Zhu, E. W. Plummer, and J. Zhang, Role of disorder and correlations in the metal-insulator transition in ultrathin SrVO_3 films, *Phys. Rev. B* **100**, 155114 (2019).
- [44] X. Zhang, A. N. Penn, L. Wysocki, Z. Zhang, P. H. M. Van Loosdrecht, L. Kornblum, J. M. Lebeau, I. Lindfors-Vrejoiu, and D. P. Kumah, Thickness and temperature dependence of the atomic-scale structure of SrRuO_3 thin films, *APL Mater.* **10**, 051107 (2022).
- [45] S. H. Chang, Y. J. Chang, S. Y. Jang, D. W. Jeong, C. U. Jung, Y. J. Kim, J. S. Chung, and T. W. Noh, Thickness-dependent structural phase transition of strained SrRuO_3 ultrathin films: The role of octahedral tilt, *Phys. Rev. B* **84**, 104101 (2011).
- [46] S. A. Lee, S. Oh, J. Lee, J. Y. Hwang, J. Kim, S. Park, J. S. Bae, T. E. Hong, S. Lee, S. W. Kim, W. N. Kang, and W. S. Choi, Tuning electromagnetic properties of SrRuO_3 epitaxial thin films via atomic control of cation vacancies, *Sci. Rep.* **7**, 11583 (2017).
- [47] R. Gao, Y. Dong, H. Xu, H. Zhou, Y. Yuan, V. Gopalan, C. Gao, D. D. Fong, Z. Chen, Z. Luo, and L. W. Martin, Interfacial octahedral rotation mismatch control of the symmetry and properties of SrRuO_3 , *ACS Appl. Mater. Interfaces* **8**, 14871 (2016).
- [48] P. Allen, P. Allen, T. Jarlborg, A. Junod, B. Revaz, and G. Santi, transport properties, thermodynamic properties, and electronic structure of SrRuO_3 , *Phys. Rev. B* **53**, 4393 (1996).
- [49] G. Koster, L. Klein, W. Siemons, G. Rijnders, J. S. Dodge, C.-B. Eom, D. H. A. Blank, and M. R. Beasley, Structure, physical properties, and applications of SrRuO_3 , *Rev. Mod. Phys.* **84**, 253 (2012).
- [50] A. Biswas, K.-S. Kim, and Y. H. Jeong, Metal insulator transitions in perovskite SrIrO_3 thin films, *J. Appl. Phys.* **116**, 213704 (2014).
- [51] L. Chen, Z. Wang, G. Wang, H. Guo, M. Saghayezhian, Z. Liao, Y. Zhu, E. W. Plummer, and J. Zhang, Surface and interface properties of $\text{La}_{2/3}\text{Sr}_{1/3}\text{MnO}_3$ thin films on SrTiO_3 (001), *Phys. Rev. Mater.* **3**, 044407 (2019).
- [52] Z. Liao, F. Li, P. Gao, L. Li, J. Guo, X. Pan, R. Jin, E. W. Plummer, and J. Zhang, Origin of the metal-insulator transition in ultrathin films of $\text{La}_{2/3}\text{Sr}_{1/3}\text{MnO}_3$, *Phys. Rev. B* **92**, 125123 (2015).
- [53] P. A. Lee and T. V. Ramakrishnan, Disordered electronic systems, *Rev. Mod. Phys.* **57**, 287 (1985).
- [54] Z. Ali, D. Basaula, K. F. Eid, and M. Khan, Anisotropic properties of oblique angle deposited permalloy thin films, *Thin. Solid. Films* **735**, 138899 (2021).
- [55] Z. Ali, *Growth, Transport, and Magnetic Properties of Oblique-Angle-Deposited Permalloy Thin Films* (Miami University, Miami, 2018).
- [56] M. Verissimo-Alves, P. García-Fernández, D. I. Bilc, P. Ghosez, and J. Junquera, Highly Confined Spin-Polarized

- Two-Dimensional Electron Gas in SrTiO₃/SrRuO₃ Superlattices, *Phys. Rev. Lett.* **108**, 107003 (2012).
- [57] G. Bergmann, Weak localization in thin films: A time-of-flight experiment with conduction electrons, *Phys. Rep.* **107**, 1 (1984).
- [58] P. A. Lee and T. V. Ramakrishnan, Magnetoresistance of weakly disordered electrons, *Phys. Rev. B* **26**, 4009 (1982).
- [59] Z. Ali, D. Basaula, W. Zhou, J. Brock, M. Khan, and K. F. Eid, Controlling the charge transport mode in permalloy films using oblique angle deposition, *J. Magn. Magn. Mater.* **484**, 430 (2019).
- [60] B. I. Shklovskii and A. L. Efros, *Electronic Properties of Doped Semiconductors*, Vol. 45 (Springer, Berlin, 1984).
- [61] V. F. Gantmakher and L. I. Man, *Electrons and Disorder in Solids* (Oxford University Press, Oxford, 2005).
- [62] P. W. Anderson, Absence of diffusion in certain random lattices, *Phys. Rev.* **109**, 1492 (1958).
- [63] T. Ying, Y. Gu, X. Chen, X. Wang, S. Jin, L. Zhao, W. Zhang, and X. Chen, anderson localization of electrons in single crystals: Li_xFe₇Se₈, *Sci. Adv.* **2**, e150123 (2016).
- [64] W. Siemons, G. Koster, A. Vailionis, H. Yamamoto, D. H. A. Blank, and M. R. Beasley, Dependence of the electronic structure of SrRuO₃ and its degree of correlation on cation off-stoichiometry, *Phys. Rev. B* **76**, 075126 (2007).
- [65] H. G. Lee, L. Wang, L. Si, X. He, D. G. Porter, J. R. Kim, E. K. Ko, J. Kim, S. M. Park, B. Kim, A. T. S. Wee, A. Bombardi, Z. Zhong, and T. W. Noh, Atomic-scale metal-insulator transition in SrRuO₃ ultrathin films triggered by surface termination conversion, *Adv. Mater.* **32**, 1905815 (2020).
- [66] L. Capogna, A. P. Mackenzie, A. P. Mackenzie, R. S. Perry, S. A. Grigera, L. M. Galvin, P. Raychaudhuri, A. J. Schofield, C. S. Alexander, G. Cao, S. R. Julian, and Y. Maeno, Sensitivity to Disorder of the Metallic State in the Ruthenates, *Phys. Rev. Lett.* **88**, 076602 (2002).
- [67] Y. K. Wakabayashi, S. Kaneta-Takada, Y. Krockenberger, K. Takiguchi, S. Ohya, M. Tanaka, Y. Taniyasu, and H. Yamamoto, Structural and transport properties of highly Ru-deficient SrRu_{0.7}O₃ thin films prepared by molecular beam epitaxy: Comparison with stoichiometric SrRuO₃, *AIP Adv.* **11**, 035226 (2021).
- [68] H. Jeong, S. G. Jeong, A. Y. Mohamed, M. Lee, W. S. Noh, Y. Kim, J. S. Bae, W. S. Choi, and D. Y. Cho, Thickness-dependent orbital hybridization in ultrathin SrRuO₃ epitaxial films, *Appl. Phys. Lett.* **115**, 092906 (2019).
- [69] S. Kunkemöller, K. Jenni, D. Gorkov, A. Stunault, S. Streltsov, and M. Braden, Magnetization density distribution in the metallic ferromagnet SrRuO₃ determined by polarized neutron diffraction, *Phys. Rev. B* **100**, 054413 (2019).
- [70] D. Toyota, I. Ohkubo, H. Kumigashira, M. Oshima, T. Ohnishi, M. Lippmaa, M. Kawasaki, and H. Koinuma, Ferromagnetism stabilization of ultrathin SrRuO₃ films: Thickness-dependent physical properties, *J. Appl. Phys.* **99**, 8 (2006).